

Exploring Ductal Carcinoma In-Situ to Invasive Ductal Carcinoma Transitions Using Energy Minimization Principles

M.V. Sheraton^{1,2,3,†*}, S. Ma^{4,†}

¹HEALTHTECH NTU, Interdisciplinary Graduate School, Nanyang Technological University, Singapore

²Institute for Advanced Study, University of Amsterdam, The Netherlands

³Center for Experimental and Molecular Medicine, Amsterdam UMC location University of Amsterdam

⁴School of Chemical and Biomedical Engineering, Nanyang Technological University, Singapore

v.s.muniraj@uva.nl

*corresponding author

Abstract. Ductal carcinoma in-situ (DCIS) presents a risk of transformation to malignant intraductal carcinoma (IDC) of the breast. Three tumor suppressor genes *RB*, *BRCA1* and *TP53* are critical in curtailing the progress of DCIS to IDC. The complex transition process from DCIS to IDC involves acquisition of intracellular genomic aberrations and consequent changes in phenotypic characteristics and protein expression level of the cells. The spatiotemporal dynamics associated with breach of epithelial basement membrane and subsequent invasion of stromal tissues during the transition is less understood. We explore the emergence of invasive behavior in benign tumors, emanating from altered expression levels of the three critical genes. A multiscale mechanistic model based on Glazier-Graner-Hogeweg method-based modelling (GGH) is used to unravel the phenotypical and biophysical dynamics promoting the invasive nature of DCIS. Ductal morphologies including comedo, hyperplasia and DCIS, evolve spontaneously from the interplay between the gene activity parameters in the simulations. The spatiotemporal model elucidates the cause-and-effect relationship between cell-level biological signaling and tissue-level biophysical response in the ductal microenvironment. The model predicts that *BRCA1* mutations will act as a facilitator for DCIS to IDC transitions while mutations in *RB* act as initiator of such transitions.

Keywords: Glazier-Graner-Hogeweg model, BRCA1, ductal morphologies

1 Introduction

Mutations in the intraductal epithelial cells of the mammary gland result in unrestrained proliferation of the cells resulting in ductal carcinoma in situ (DCIS) (1). This condition is classified as a non-invasive lesion. These epithelial cells are confined within the lumen and therefore are restrained from spreading outside the duct to the surrounding tissues. Further progression of DCIS and disruption of the basal membrane

results in malignant condition known as invasive ductal carcinoma (IDC) (2). After the onset of IDC, the cancer cells invade other parts of the breast tissue and turn metastatic. Transformation from DCIS to life threatening IDC has long been a subject of clinical research (3-5). Studies have suggested that DCIS is a precursor for IDC and on average 40% of patients with DCIS subsequently develop IDC (6). Luminal B1 tumors (7) have shown faster progression from DCIS to IDC than luminal A, triple negative and HER2 type tumors. HER2 positive tumors are found to transit from DCIS to IDC slower by staying in the DCIS state longer. Though, specific pathways and biomarkers for this transformation are yet to be discovered. Logullo et al. (8) analyzed epithelial to mesenchymal transition (EMT) markers for their association with DCIS to IDC transformation and found that c-met and TGF β 1 had positive association with the tumor transformation. However, most EMT biomarkers did not yield significant prognosis value. One important characteristic associated with IDC is the presence of intra-tumor morphological and genetic heterogeneity. “Evolutionary bottleneck” was suggested as an outcome of progression from DCIS to IDC by Cowell et al. (2), to explain the genetic heterogeneity observed in IDCs. This transformation is a complex process involving multiple mutations resulting in a highly heterogenous tumor microenvironment. p53 overexpression (9) has been observed in both DCIS and IDC, with the overexpression leading to lower mitotic index and apoptotic index in luminal cell phenotype and the opposite in stem cell phenotype. There is evidence (10, 11) suggesting that DCIS lesions and IDC tumors have deactivated the retinoblastoma gene, ie., loss of Rb function and that the Rb pathway is a likely regulator of the transformations. Rb has also been shown to be a deciding factor in the recurrence of DCIS (11) through overexpression of p16ink4a. Mutations in the *BRCA* genes (the tumor suppressor gene widely associated with breast cancer) and the gene encoding p53 (*TP53*) have been found to occur together in both DCIS and IDC tumors (12). Kumar et al. (13) studied the combined effect of the defects of these three major tumor suppressors genes, *RB*, *BRCA1* and *TP53*. They observed that simultaneous deactivation of these pathways resulted in formation of highly metastatic invasive breast cancer tumors in their mouse models and concluded that the pathways have a combinatorial effect on the progress and evolution of the tumor growth. The resulting tumors were found to have heterogenous morphology suggesting a product of “Evolutionary bottleneck” similar to studies of Cowell et al. (2) Thus, alterations in these three pathways would result in formation of highly invasive tumors and could possibly act as precursors in DCIS to IDC transformations.

Histological staining of tissue sections is traditionally used to study DCIS-IDC transformation, yet it is rather difficult to understand the complexities associated with the disease and it is less feasible to design experiments to track the progress of tumor evolution. Computational modelling of biological cells has become a useful tool in predicting the outcome of tumor growth, angiogenesis, and tissue morphologies in-silico (14, 15). Multiscale agent based models have been accepted widely due to their versatility in handling multiple cell phenotypes and therefore tissue heterogeneity (16, 17). Qiao et al. (18) developed an agent based model to simulate the proliferation of multiple myeloma tumor cells and analyzed the effect of drugs on the population of osteoclasts and osteoblasts. They modelled cells as agents and drugs as apoptosis inducers. The cells were modelled to undergo apoptosis at variable rates based on the quantity of

drugs they are in contact with. The effect of tyrosine inhibitor kinases (TKIs) on brain cancer was studied using a similar multiscale model by Sun et al. (19) They incorporated EGFR signaling in their model using partial differential equations to simulate various phenotypes observed in the tumor. The developmental stages of DCIS also have been simulated using agent-based modeling. The model developed by Macklin et al. (20) was able to provide insight into the formation of necrotic core and calcification regions. Though these models can quantify the tumor proliferation and apoptosis, they lack proper energy based realistic cell allocations from mitosis or cell motility. These mesoscale interactions determine the spatial distribution and localized effects associated with the position of tumor cells. A better way of modelling the cells in an energy optimistic way with cell motility while retaining the individual characteristics of cells is through Glazier-Graner-Hogeweg method-based modelling (GGH). Boghaert et al. (21) used GGH to simulate the progression of DCIS growth. Due to the inherent energy minimization principle of GGH, they were able to simulate four different forms of DCIS morphologies, namely micropapillary, cribriform, solid and comedo. These morphologies would not have evolved in other agent-based models due to the absence of localized energy interactions. However, the model was unable to predict beyond the transition from DCIS to IDC and explain the reasons for the observed phenotypic heterogeneity in the clinical IDC sections.

In this study, we use GGH to develop a model to elucidate on the transition from DCIS and IDC stage. We consider the critical three tumor suppressor pathways involving p53, Rb and BRCA to simulate the phenotypic variations associated with the underlying genotypic changes. We make valid assumptions based on available literature data to interpret the effects of genotypic changes into physical model parameters. By combining phenotypic changes, genotypic influences on cell proliferation and energy minimization principles we model the intraductal luminal epithelial cells and myoepithelial cells to elaborate the mechanism of DCIS to IDC transformation and the associated morphological heterogeneity.

2 Methods and Materials

2.1 Model description

Two basic cell types, epithelial cells and myoepithelial cells were modeled. The former cell type forms the inner layer and the latter stays along the periphery as shown in figure 1. Individual cells were modelled as collection of lattice points on the simulation grid. The Glazier-Graner-Hogeweg (GGH) method-based model was implemented using an open-source software framework called CompuCell3D v3.7.5. The developed method is an extension of the model developed by Boghaert et al. (21) to simulate DCIS. The cells in the simulation are free to deform based on the energy constraints listed in equation 1 at each monte-carlo step (mcs). The cells deform at lattice point level through lattice point-copy attempts (22). The probability of success for a lattice point copy attempt is defined by equation one, where, $\sigma(\vec{i})$ denotes the lattice point

occupied by a cell σ , \vec{i}' represents the new lattice point where the lattice point copy attempt is supposed occur, ΔH is the change in energy of the system and T_m is the temperature or fluctuation amplitude of the system. The lattice point-level deformations, on a longer time scale, constitute the motility of the cells. Volume constraints were imposed on the cells to ensure that the cells stay within permissible levels of volume increase or decrease using equation 2. The term E_v denotes the volume energy of the cell, V_{cell} denotes the total number of lattice points occupied by the cell, V_T denotes the target volume of the cell and λ_v denotes the volume potential (similar to a spring constant). A surface area constraint was introduced in the model to prevent the cells from evolving into biologically unreasonable shapes. The terms E_s , S_{cell} , S_T and λ_s denote the surface energy, total number of lattice points on the surface (perimeter in 2D), target surface area and the surface potential respectively. In addition, to restrict the cells from disintegrating and assuming fractured morphologies, a penalty function E_p was imposed (23). This parameter retains individual cells as a single entity. The focal point plasticity (FPP) of the cell and contact energies between the cells are dictated by the equations 4 and 5. Here, l_{ij} is the distance between cells at positions i and j , L_{ij} is the target distance between the cells, and λ_{ij} is the FPP potential. We used the physically equivalent values as suggested by Boghaert et al. (21), to simulate the cells' attraction-repulsion potential and adhesion forces. The energy arising from a lattice point copy attempt 'H' is therefore given by equation 6. We assume the cells to be spherical with a diameter of 15 μm .

$$P(\sigma(\vec{i}) \rightarrow \sigma(\vec{i}')) = \begin{cases} \left[\exp\left(-\frac{\Delta H}{T_m}\right) \right], & \Delta H > 0 \\ 1, & \Delta H \leq 0 \end{cases} \quad (1)$$

$$E_v = \sum_{\sigma} \lambda_v (V_{\text{cell}}(\sigma) - V_T(\sigma))^2 \quad (2)$$

$$E_s = \sum_{\sigma} \lambda_s (S_{\text{cell}}(\sigma) - S_T(\sigma))^2 \quad (3)$$

$$E_c = \sum_{i,j} J(\tau_{\sigma(i)}, \tau_{\sigma(j)}) (1 - \delta_{\sigma(i), \sigma(j)}) \quad (4)$$

$$E_f = \sum_{i,j} \lambda_{i,j} (l_{i,j} - L_{i,j})^2 \quad (5)$$

$$H = E_v + E_s + E_c + E_f \quad (6)$$

Each cell has three major biological parameters associated with it, the DNA damage level, oxidative stress, and proliferation potential. All these biological parameters were modelled as non-dimensional continuous variables from 0 to 1.0. Equation 6 describes the change in DNA damage level within the cells. Cells accumulate DNA damage 'd' in a stochastic manner with a probability f_{dd} (24) as shown in equation 7.

C_B indicates the expression level of BRCA. The proliferation potential ‘ p ’ was assumed to decrease with increase in number of epithelial neighbors, since a crowded microenvironment would result in less nutrient available for cell growth. To calculate the number of neighbors, we used a neighbor order of 1.5 times the cell radius for epithelial (N_e) and myoepithelial cell neighbors (N_m). Also, the proliferation potential was modelled to increase with DNA damage accumulated in the cancer cells. The increased proliferation potential of a DNA damaged cell can be considered as an inherent property of a mutated cell with higher survivability capacity (25). Proliferation potential was calculated using equation 8. Where, β , k_{os} , C_{Rb} and O represent specific growth rate, oxidative stress coefficient and oxidative stress respectively. The oxidative stress within the cells was assumed to increase from crowding of cell neighbors (decrease in nutrient availability) and the cell type of these neighbors (26). Epithelial contribution to oxidative stress was considered to be negligible for a cell with fewer than 5 neighbors. The oxidative stress contribution from myoepithelial neighbors was also considered to reduce with increase in number of neighbors as dictated by equation 9. This assumption is based on the ready availability nutrient for epithelial cells that are located near myoepithelial cells, as observed by Norton et al. (27). In equation 9, the constants ω_1 and ω_2 are the weighting fractions for oxidative stress contribution from the two types of neighbor cells, W is the maximum contribution to oxidative stress from the neighbors and ‘ a ’ stress generation rate coefficient.

The gene activity and protein expression levels control the cell cycle by indirectly controlling the three major cell survivability parameters. RB functions as a tumor suppressor gene by being a negative regulator of cell proliferation. Cells which have suffered DNA damage or accumulated oxidative stress are arrested in their G1 phase by the activity of RB (28). In our model, this gene activity is modelled by considering Rb (Rb protein or pRb) as a regulator of cell proliferation potential. Thus, in the simulation, Rb reduces and eventually prevents the proliferation of cells that have accumulated DNA damage and oxidative stress as defined in equation 8. The extent of Rb effect is dependent on its activity potential in the cell ‘ C_{Rb} ’.

In normal cells, the DNA damage must be limited to avoid run-off cell proliferations. Proliferation reduction in DNA damaged cells is handled by BRCA which is involved in DNA repair (29). In cases of breast cancer, the inactivation of BRCA genes have been the major reason for DNA damage and accumulation of multiple mutations. We therefore modelled BRCA activity ‘CB’ as a modifier of the DNA damage levels in the cells as shown in equation 7.

If the DNA damage or oxidative stress in cells exceed a critical level, then apoptosis is initiated based on the lethal cell DNA damage level (d_l) and probability dictated by the effectivity of p53 (C_{p53}) (30) respectively. Cells with apoptosis index ‘ I_A ’ values larger than maximum cell apoptotic index value ‘ I_{Ac} ’ are marked for removal from the simulation domain. These cells are removed if they continue to express I_A values greater than I_{Ac} for more than ‘ N_A ’ simulation time steps. Similarly, in case of mitosis, cells divide in simulation if the mitosis index ‘ I_M ’ (equation 11) is higher than the maximum cell mitotic index value ‘ I_{Mc} ’

$$d = f_{dd}[1 - C_B] \quad (7)$$

$$\frac{dp}{dt} = \beta(1 - k_{os} C_{Rb} O + C_{Rb} d), \text{ with } \max(p) = 1.0 \quad (8)$$

$$\frac{dO}{dt} = \begin{cases} W[\omega_1 e^{-aN_m} + \omega_2(1 - e^{-a(N_e - N_{max})})], & \text{if } N_e \geq N_{max} \\ W[\omega_1 e^{-aN_m}], & \text{else} \end{cases}, \text{ with } \max(O) = 1.0 \quad (9)$$

$$I_A = O * C_{p53} \quad (10)$$

$$I_M = p * C_{p53} \quad (11)$$

The cells were allowed to evolve based on the constraints dictated by equation 6 throughout the simulation. The calculations based on activity level equations 7 to 11 were computed for every 100 mcs. This cycle ensures that the cells relax for sufficient time after their growth, thereby, assuring minimal energy state of the system. Each 100 mcs corresponds to 0.25 hours real time. The simulations were carried out for a maximum of 100000 mcs (250 hours) or until the maximum cell count in the simulations reached 1000, whichever event occurred earlier. Parametric values used in the simulations are summarized in table 1.

3 Results and Discussions

The model simulations with maximum levels (1.0) of C_B , C_{p53} and C_{Rb} should result in a normal ductal structure. Maximum levels of activity should prevent apoptosis evasion or proliferation runoff of the cells. These structures should possess a single layer of myoepithelial cells enclosing one or two layers of epithelial cell with minimal distortions to ductal morphology. Ensuring that the model establishes and maintains the above-mentioned structure throughout the simulation duration is the first step in verifying if the model assumptions represent in-vivo dynamics. As hypothesized, the simulations carried out with maximum expression levels are found to produce benign normal ductal structures as shown in figure 1a. The structure is found to be in a dynamic equilibrium. Meaning, the aging cells are removed with simulation progress and are replaced by new daughter cells. This cycle repeats itself throughout the entire simulation duration. The variation in formation of new cells and live epithelial cell count during the course of simulation for this case are shown in figure 1b and 1c respectively. The intertwined effects of apoptosis and mitosis can be seen to regulate the ductal level cell population homeostasis. Thus, the simulations capture the in-vivo co-operative effect of BRCA, RB and P53 on the regulation of ductal development and functioning. A cell-field plot of oxidative stress levels is presented in figure 1d. Oxidative stress levels are found to vary throughout the entire structure suggesting the absence of localized overcrowding in these structures. The plots also capture the elimination of any cells that have accumulated critical oxidative stress. The major fixed parameters used in the study, W and β play a crucial role in establishing this mitosis and apoptosis balance. The value of W was chosen in such a way that in the absence of DNA damage and oxidative stress, on average the cells divide around every 17 hours. This proliferation duration is similar to those reported in experimental studies (31, 32). β -value is an

analog of W -value for oxidative stress, both these values were quantitatively set to be equal. Hence, the dynamic equilibrium established between the proliferation-apoptosis cycle is driven by the perturbations arising from the oxidative contributions of the neighboring cells. Figure 1e shows the normalized duration since the last cell division, which closely follows the trend of oxidative stress levels with the cells.

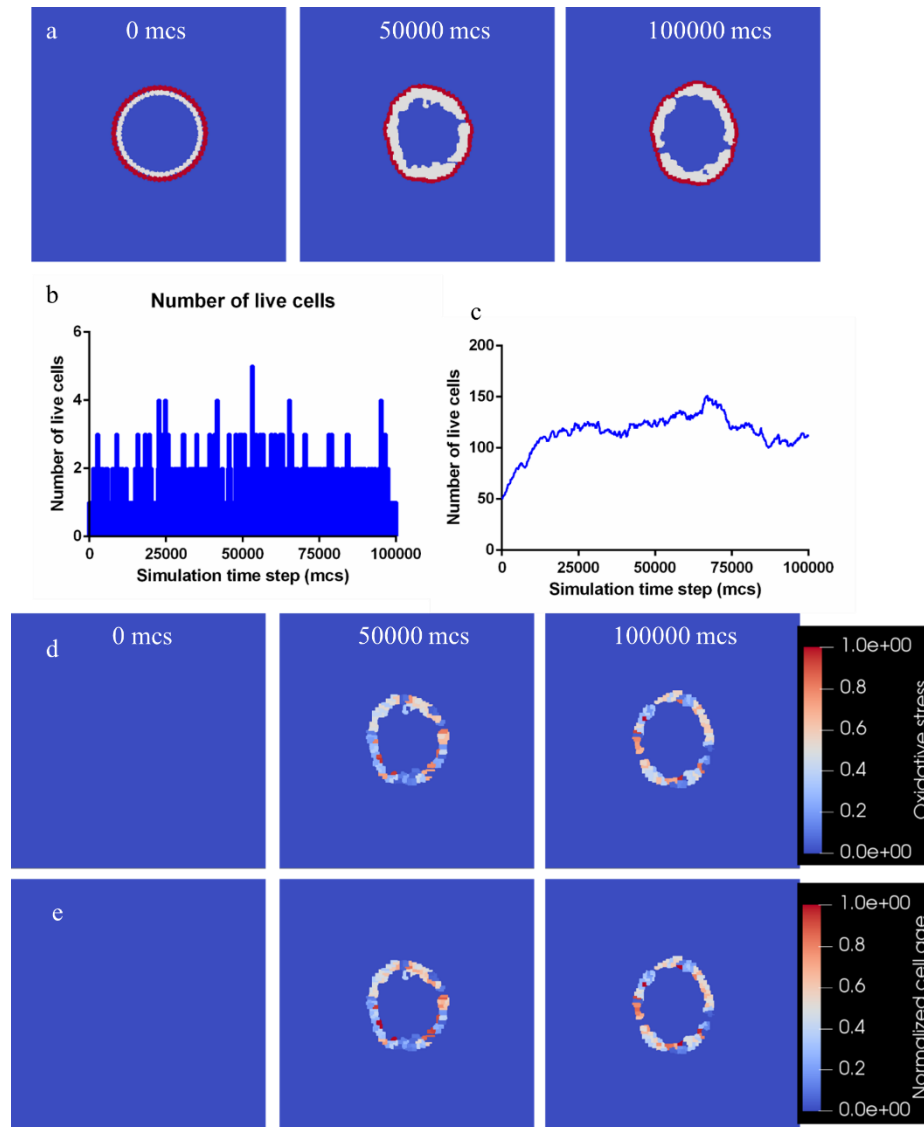


Fig. 1. Model simulation results for normal ductal structure formation at maximum (1.0) C_B , C_{p53} and C_{Rb} values. (a) Panel showing spatial changes in ductal structure (white color indicates epithelial cells and red color indicates myoepithelial cells) at 0, 50000 and 100000 mcs, (b) temporal variations in number of new cell formations, (c) temporal variations in total epithelial cell

count, panel showing spatial variations of (d) oxidative stress and (e) normalized cell age at 0, 50000 and 100000 mcs.

On an average all the cells in the simulation were replaced every 8500 mcs (21.25 hours). This novel dynamic replacement behavior is more realistic than previous DCIS models in literature (21, 27). These models used a stochastic way of apoptosis, where in a cell in the simulation domain was picked randomly at fixed intervals and removed based on probability outcomes. These methods introduced a model artifact of ‘irreplaceable cells’ which are never removed from the simulation domain. Our approach eliminates these cells and closely mimics the in-vivo mechanism of replacement of damaged aging cells with new cells. The values of C_B , C_{p53} and C_{Rb} were varied from 0.25 to 1.0 in increments of 0.25 in a combined manner in the simulations. Figure 2a shows the number of cases with less than 125 surviving cells at the end of simulations. These cases, in general, produce a ductal configuration very similar to the normal state, that is, a single layer of myoepithelial cells binding fewer than three layers of epithelial cells. The x-axis in figure 2a denotes the cases where the values of C_B , C_{p53} and C_{Rb} were kept maximum (1.0). As observed, simulations with maximum values of C_{Rb} tend to produce most controlled growth of epithelial cells. Even though Rb was not modelled as a direct influencer of apoptosis, it is found to be a major driver of cell aging control. This simulation result also correlates with other experimental observations where lower Rb expression levels have been implicated with risk of ipsilateral breast event (IBE) (33) and DCIS to IDC transformations (10, 11). It should be noted that there are other cases where even with maximum expression of Rb, the cells proliferated in an uncontrolled manner. This means that C_{Rb} is not the sole controlled of apoptosis-mitosis equilibrium.

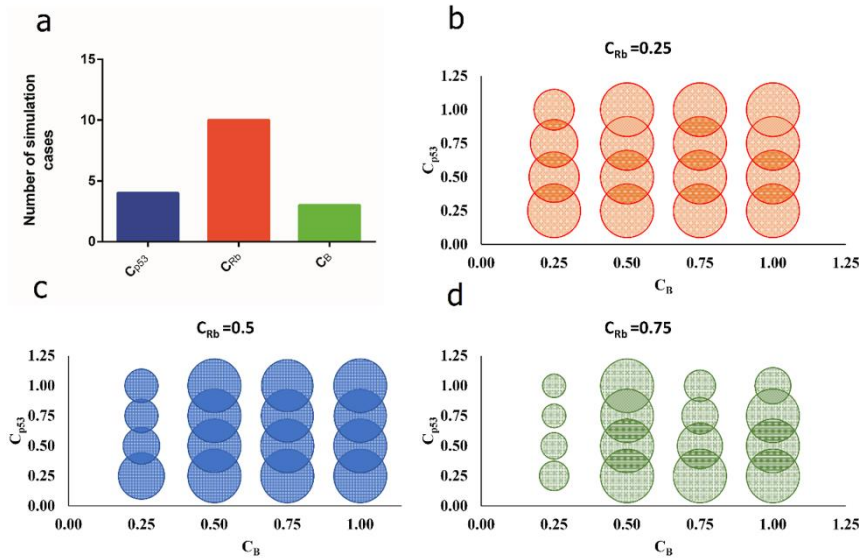


Fig. 2. Variation of cell count for different parametric values. (a) Number of cases with cell count less than 125 and maximum parameter values (1.0) Total cell count at the end of simulations for different values of C_{p53} and C_B and fixed value C_{Rb} of (b) 0.25, (c) 0.5 and (d) 0.75. The circle size indicates the number of cells, with maximum cell count (1000) corresponding to the maximum circle diameter.

To further unravel the intertwined effects of C_B and C_{p53} , 2D density plots of cell counts for various fixed values of C_{Rb} are used as shown in figure 2b,2c and 2d. It can be observed that for fixed values of $C_{Rb}=0.5$ and 0.75 , reduced cell population levels are seen for C_{p53} value of 0.25 , irrespective of the C_B value. These values are lower than their counterparts with C_{p53} values 0.5 and 0.75 . This outcome is unexpected since a reduced C_{p53} value would mean more chances of cell survival as dictated by equation 10. Although counterintuitive, this observation can be attributed to the decreased levels of both apoptotic and mitotic indices of these cells (I_A and I_M) at minimum C_{p53} value. This results in a pathway-race between proliferation and apoptosis. Hence, for fixed values of C_{Rb} at 0.5 and 0.75 , effect of apoptosis is more pronounced in simulations with C_{Rb} value of 0.25 than simulations with C_{Rb} values greater than 0.25 . The above observations do not hold true for simulations with fixed C_{Rb} and C_{p53} values of 1.0 and 0.5 respectively. In these cases, the total live cell population is found to be lower than simulations with fixed C_{Rb} of 1.0 and C_{p53} values of other than 0.5 . Interestingly, simulations with C_{p53} value of 0.5 are the only simulations with more than 150 cells at maximum C_{Rb} expression levels. Thus, the system produces non-linear response to C_{p53} effectivity levels and the outcomes are dependent on the interplay of all three parameters (C_{p53} , C_{Rb} and A_B).

Heightened levels of cell proliferation and survival alone cannot be considered as indicators of invasive transformations. Elevated proliferation and cell survival are characteristics of both DCIS and IDC tumors. To be characterized invasive, the epithelial cell populations should proliferate enough to fill the space between the ducts and penetrate the myoepithelial layer to invade surrounding tissues. The simulation results were examined for morphological differences arising from variations in the activity parameters. Four unique ductal structures were obtained from the parametric simulation studies. The structures are shown in figure 3a-3d. They can be classified as (1) normal ductal configuration, (2) ductal hyperplasia, (3) solid or comedo and (4) invasive ductal configuration. The spatial development of these configurations is shown in figure 3a-3d respectively. In ductal hyperplasia structures (fig. 3b), layers of epithelial cells are found to extend from the myoepithelial wall towards the ductal core. Such structures are generally categorized as benign in-vivo. However, they are considered as risk factors for breast cancer development. Further uncontrolled proliferation of cells in hyperplasia structures will result in formation of solid or comedo structures such as the one shown in figure 3c. These structures are categorized as high-grade DCIS. If left untreated these structures can progress to invasive ductal carcinoma. Figure 3d shows the invasive ductal carcinoma formed in simulation. The major difference between solid and invasive structures is the presence of cells that have penetrated the myoepithelial layer. Invasive ductal carcinoma (IDC) structures are malignant in nature, after penetration, the IDC cells invade the local tissue and establish a population there. In most

simulation cases, the penetration of cells is aided by the intraductal pressure or energy build up. This energy build-up makes the myoepithelial chain unstable resulting in local adhesion failures and epithelial cell break away.

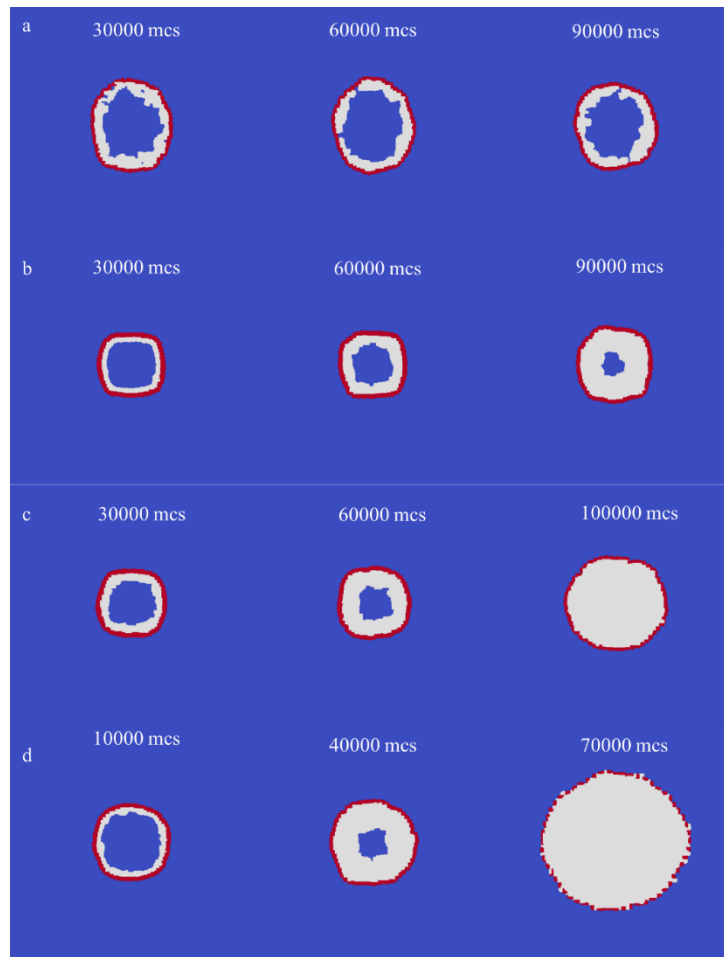


Fig. 1. Ductal structures formed during the simulations. (a) Formation of normal duct structure with parameter values of $C_B = 1$, $C_{p53} = 1$ and $C_{Rb} = 1$, (b) formation of ductal hyperplasia structure with parameter values of $C_B = 1$, $C_{p53} = 0.25$ and $C_{Rb} = 0.75$, (c) formation of solid structure with parameter values of $C_B = 1$, $C_{p53} = 0.25$ and $C_{Rb} = 0.5$ and (d) formation of invasive ductal carcinoma structure with parameter values of $C_B = 0.25$, $C_{p53} = 0.5$ and $C_{Rb} = 0.75$. The white spots indicate epithelial cells and red spots indicate myoepithelial cells.

Multiple structures can form for a single value of C_B , C_{p53} and C_{Rb} parameter in the parametric combinations. To better understand the contribution of each of these values towards formation of different ductal structures, figure 4 summarizes the number of instances of formation of various structures at different expression levels. Conclusively,

all variational combinations are found to predominantly produce IDC structure. This means DCIS to IDC transformations are possible from all variations in C_{p53} and C_{Rb} . From simulation data, for the case of variations in C_B values, IDC transformations are possible only if coupled with variation in expression levels of other parameters. This observation suggests a promotional role for BRCA in IDC transformations rather than as an initiator. C_{Rb} is found to produce most of the normal ductal structures in the simulation at the maximum expression level. Therefore, Rb should act as a major restraint in DCIS to IDC transformations. In addition, minimum level $C_{Rb}(0.25)$ is found to solely produce IDC structures. This shows the crucial effect of C_{Rb} reduction on formation of IDC structures. The non-linear nature of the responses evoked from C_{p53} variations is further evident in figure 4c. p53 effectivity level of 0.5 is found to produce solely of IDC structures. The number of structures produced at this effectivity level is even higher than the number of structures produced at a lower effectivity level of 0.25. As previously discussed, this phenomenon can be attributed to the pathway-race condition between apoptosis and cell proliferation.

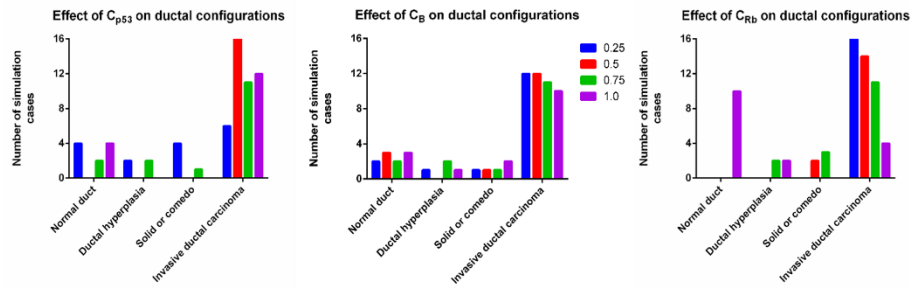


Fig. 2. Formation of various ductal structures for different values of C_B , C_{p53} and C_{Rb} . The color legend indicates various activity levels of the simulation parameters.

Table 1. Key parametric values used in the simulations

Parameter	Notation	Value (units)
Time step	mcs	2.5×10^{-3} (h)
Volume potential	λ_v	5 - 10
Surface potential	λ_s	2
Temperature	T_m	10
DNA damage probability	f_{dd}	0.5
Oxidative stress contribution from myoepithelial neighbors	ω_1	0.75
Oxidative stress contribution from epithelial neighbors	ω_2	0.25
Maximum neighbors	N_{max}	5
Oxidative stress coefficient	k_{os}	0.67

4 Conclusions

We developed a GGH method-based model for simulating the biological and biophysical interactions occurring between cells in the mammary ducts. The numerical model was used to explore the effects of mutation of three major tumor suppressor genes (RB, TP53 and BRCA1) on the ductal microenvironment. Through the model simulations, we captured the spatiotemporal changes occurring in the tumor microenvironment, which are instigated by the altered gene expression levels in the ductal cells. The developed model has captured the dynamics of development of various ductal structures. These structures include normal duct, ductal hyperplasia, comedo and invasive ductal carcinoma structure. Cells in the simulations were replaced periodically by new cells similar to in-vivo tissue cell population homeostasis. DCIS to IDC transformation is found to be initiated through variations in expression levels and effectivity of Rb and p53 respectively. The model simulations suggest a promoter role for BRCA in progression from DCIS to IDC. In a word, our model simulates the transformation of DCIS to IDC of breast cancer, and demonstrates the influence of impaired activities of BRCA, RB and P53 on such transitions.

Gene sequencing techniques and clinical sample processing methods have advanced dramatically in recent years. Technologies including microarray, next generation sequencing and ddPCR enable clinicians and scientists to detect mutations and expression levels of thousands of genes from liquid biopsy or tissues samples of patients. However, the lack of efficient analysis tools and modeling systems limits our understanding of the sequencing and detection data. Here we have developed a numerical model to simulate the combinational influence of BRCA, Rb and p53 activities on DCIS to IDC transformation. Our model could be used to analyze the mutation status and expression levels of BRCA, Rb and p53, to predict the disease progression and survival of patients. Drugs that directly target BRCA, Rb and p53 or inhibit the related pathways have been approved for breast cancer treatment, such as Palbociclib, Ribociclib and Olaparib. The simulation model can act as a tool for experimental hypotheses testing. Based on the mutations and expression data of the genes, further development would enable gene expression data-driven personalized selective inhibitor drug scheduling.

5 References

1. Gorringer, K.L., Fox, S.B.: Ductal Carcinoma In Situ Biology, Biomarkers, and Diagnosis. *Front Oncol* 7, 248 (2017)
2. Cowell, C.F., Weigelt, B., Sakr, R.A., Ng, C.K., Hicks, J., King, T.A., Reis-Filho, J.S.: Progression from ductal carcinoma in situ to invasive breast cancer: revisited. *Mol Oncol* 7, 859-869 (2013)

3. Ma, X.-J., Salunga, R., Tuggle, J.T., Gaudet, J., Enright, E., McQuary, P., Payette, T., Pistone, M., Stecker, K., Zhang, B.M.: Gene expression profiles of human breast cancer progression. *Proceedings of the National Academy of Sciences* 100, 5974-5979 (2003)
4. Aubele, M.M., Cummings, M.C., Mattis, A.E., Zitzelsberger, H.F., Walch, A.K., Kremer, M., Höfler, H., Werner, M.: Accumulation of chromosomal imbalances from intraductal proliferative lesions to adjacent in situ and invasive ductal breast cancer. *Diagnostic Molecular Pathology* 9, 14-19 (2000)
5. Volinia, S., Galasso, M., Sana, M.E., Wise, T.F., Palatini, J., Huebner, K., Croce, C.M.: Breast cancer signatures for invasiveness and prognosis defined by deep sequencing of microRNA. *Proceedings of the National Academy of Sciences* 109, 3024-3029 (2012)
6. Boughey, J.C., Gonzalez, R.J., Bonner, E., Kuerer, H.M.: Current treatment and clinical trial developments for ductal carcinoma in situ of the breast. *The oncologist* 12, 1276-1287 (2007)
7. Kurbel, S., Marjanović, K., Dmitrović, B.: A model of immunohistochemical differences between invasive breast cancers and DCIS lesions tested on a consecutive case series of 1248 patients. *Theoretical Biology and Medical Modelling* 11, 29 (2014)
8. Brentani: Concomitant expression of epithelial-mesenchymal transition biomarkers in breast ductal carcinoma: Association with progression. *Oncology Reports* 23, (2009)
9. Megha, T., Ferrari, F., Benvenuto, A., Bellan, C., Lalinga, A., Lazzi, S., Bartolommei, S., Cevenini, G., Leoncini, L., Tosi, P.: p53 mutation in breast cancer. Correlation with cell kinetics and cell of origin. *Journal of clinical pathology* 55, 461-466 (2002)
10. Gauthier, M.L., Berman, H.K., Miller, C., Kozakeiwicz, K., Chew, K., Moore, D., Rabban, J., Chen, Y.Y., Kerlikowske, K., Tlsty, T.D.: Abrogated response to cellular stress identifies DCIS associated with subsequent tumor events and defines basal-like breast tumors. *Cancer Cell* 12, 479-491 (2007)
11. Witkiewicz, A.K., Rivadeneira, D.B., Ertel, A., Kline, J., Hyslop, T., Schwartz, G.F., Fortina, P., Knudsen, E.S.: Association of RB/p16-pathway perturbations with DCIS recurrence: dependence on tumor versus tissue microenvironment. *The American journal of pathology* 179, 1171-1178 (2011)
12. Wang, X., El-Halaby, A.A., Zhang, H., Yang, Q., Laughlin, T.S., Rothberg, P.G., Skinner, K., Hicks, D.G.: p53 alteration in morphologically normal/benign breast luminal cells in BRCA carriers with or without history of breast cancer. *Hum Pathol* 68, 22-25 (2017)
13. Kumar, P., Mukherjee, M., Johnson, J.P., Patel, M., Huey, B., Albertson, D.G., Simin, K.: Cooperativity of Rb, Brca1, and p53 in malignant breast cancer evolution. *PLoS genetics* 8, e1003027 (2012)
14. Palm, M.M., Merks, R.M.: Large-scale parameter studies of cell-based models of tissue morphogenesis using CompuCell3D or VirtualLeaf. *Tissue Morphogenesis: Methods and Protocols* 301-322 (2015)
15. Anderson, A.R., Chaplain, M.: Continuous and discrete mathematical models of tumor-induced angiogenesis. *Bulletin of mathematical biology* 60, 857-899 (1998)
16. Thorne, B.C., Bailey, A.M., Peirce, S.M.: Combining experiments with multi-cell agent-based modeling to study biological tissue patterning. *Briefings in bioinformatics* 8, 245-257 (2007)
17. Bailey, A.M., Thorne, B.C., Peirce, S.M.: Multi-cell agent-based simulation of the microvasculature to study the dynamics of circulating inflammatory cell trafficking. *Annals of biomedical engineering* 35, 916-936 (2007)
18. Qiao, M., Wu, D., Carey, M., Zhou, X., Zhang, L.: Multi-scale agent-based multiple myeloma cancer modeling and the related study of the balance between osteoclasts and osteoblasts. *PloS one* 10, e0143206 (2015)

19. Sun, X., Zhang, L., Tan, H., Bao, J., Strouthos, C., Zhou, X.: Multi-scale agent-based brain cancer modeling and prediction of TKI treatment response: Incorporating EGFR signaling pathway and angiogenesis. *BMC bioinformatics* 13, 218 (2012)
20. Macklin, P., Edgerton, M.E., Thompson, A.M., Cristini, V.: Patient-calibrated agent-based modelling of ductal carcinoma in situ (DCIS): from microscopic measurements to macroscopic predictions of clinical progression. *Journal of theoretical biology* 301, 122-140 (2012)
21. Boghaert, E., Radisky, D.C., Nelson, C.M.: Lattice-based model of ductal carcinoma in situ suggests rules for breast cancer progression to an invasive state. *PLoS computational biology* 10, e1003997 (2014)
22. Swat, M.H., Thomas, G.L., Belmonte, J.M., Shirinifard, A., Hmeljak, D., Glazier, J.A.: Multi-scale modeling of tissues using CompuCell3D. *Methods in cell biology* 110, 325 (2012)
23. Swat, M.H., Thomas, G.L., Belmonte, J.M., Shirinifard, A., Hmeljak, D., Glazier, J.A.: Multi-scale modeling of tissues using CompuCell3D. *Methods in cell biology*, vol. 110, pp. 325-366. Elsevier (2012)
24. Rattan, S.I.: Theories of biological aging: genes, proteins, and free radicals. *Free radical research* 40, 1230-1238 (2006)
25. Davis, J.D., Lin, S.-Y.: DNA damage and breast cancer. *World Journal of Clinical Oncology* 2, 329-338 (2011)
26. Gawel-Bęben, K., Ali, N., Ellis, V., Velasco, G., Poghosyan, Z., Ager, A., Knäuper, V.: TMEFF2 shedding is regulated by oxidative stress and mediated by ADAMs and transmembrane serine proteases implicated in prostate cancer. *Cell Biology International* n/a-n/a
27. Norton, K.-A., Popel, A.S.: An agent-based model of cancer stem cell initiated avascular tumour growth and metastasis: the effect of seeding frequency and location. *Journal of The Royal Society Interface* 11, 20140640 (2014)
28. Giacinti, C., Giordano, A.: RB and cell cycle progression. *Oncogene* 25, 5220-5227 (2006)
29. Yoshida, K., Miki, Y.: Role of BRCA1 and BRCA2 as regulators of DNA repair, transcription, and cell cycle in response to DNA damage. *Cancer science* 95, 866-871 (2004)
30. Fridman, J.S., Lowe, S.W.: Control of apoptosis by p53. *Oncogene* 22, 9030 (2003)
31. Corbin, E.A., Adeniba, O.O., Cangellaris, O.V., King, W.P., Bashir, R.: Evidence of differential mass change rates between human breast cancer cell lines in culture. *Biomedical microdevices* 19, 10 (2017)
32. Starcevic, S.L., Diotte, N.M., Zukowski, K.L., Cameron, M.J., Novak, R.F.: Oxidative DNA damage and repair in a cell lineage model of human proliferative breast disease (PBD). *Toxicological Sciences* 75, 74-81 (2003)
33. Knudsen, E.S., Pajak, T.F., Queenan, M., McClendon, A.K., Armon, B.D., Schwartz, G.F., Witkiewicz, A.K.: Retinoblastoma and phosphate and tensin homolog tumor suppressors: impact on ductal carcinoma in situ progression. *JNCI: Journal of the National Cancer Institute* 104, 1825-1836 (2012)